

## Family behavior of the optical transition energies in single-wall carbon nanotubes of smaller diameters

Ge. G. Samsonidze

*Department of Electrical Engineering and Computer Science, Massachusetts Institute of Technology, Cambridge, Massachusetts 02139-4307*

R. Saito, N. Kobayashi, A. Grüneis,<sup>a)</sup> and J. Jiang

*Department of Physics, Tohoku University and CREST JST, Aoba, Sendai 980-8578, Japan*

A. Jorio

*Departamento de Física, Universidade Federal de Minas Gerais, Belo Horizonte, MG 30123-970, Brazil*

S. G. Chou

*Department of Chemistry, Massachusetts Institute of Technology, Cambridge, Massachusetts 02139-4307*

G. Dresselhaus

*Francis Bitter Magnet Laboratory, Massachusetts Institute of Technology, Cambridge, Massachusetts 02139-4307*

M. S. Dresselhaus<sup>b)</sup>

*Department of Electrical Engineering and Computer Science and Department of Physics, Massachusetts Institute of Technology, Cambridge, Massachusetts 02139-4307*

(Received 20 July 2004; accepted 5 October 2004)

Using the extended tight-binding model that allows bond lengths and angles to vary, the optical transition energies  $E_{ii}$  in single-wall carbon nanotubes are calculated as a function of inverse tube diameter. After geometrical structure optimization, the  $2n+m=\text{constant}$  family behavior observed in photoluminescence (PL) experiments is obtained, and detailed agreement between the calculations and PL experiments is achieved after including many-body corrections. © 2004 American Institute of Physics. [DOI: 10.1063/1.1829160]

The electronic band structure of single-wall carbon nanotubes (SWNTs) is often obtained by applying the zone-folding scheme to the band structure of the graphene layer, where the latter is calculated within the tight-binding (TB) approximation.<sup>1</sup> The TB transfer and overlap integrals are then fitted to the results of experiments, such as resonance Raman scattering (RRS)<sup>2</sup> or scanning tunneling spectroscopy.<sup>3</sup> While this approach provides reliable results for larger diameter SWNTs ( $>1.2$  nm),<sup>4</sup> it fails in the smaller diameter region ( $<1.2$  nm), as has been shown recently in photoluminescence (PL) studies of SWNTs dispersed by a surfactant in an aqueous solution.<sup>5</sup> An empirical fitting approach was developed by Weisman and Bachilo to reproduce the results of the PL experiments.<sup>6</sup> In this letter, we present an extension of the zone-folding scheme and the TB approximation to the smaller diameter region which agrees well with the PL empirical fit,<sup>6</sup> thus providing a theoretical basis to account for this empirical fit that can now be safely applied to many experiments. It can also be extended to predict electronic and optical properties of SWNTs over a wider SWNT diameter and energy range, as well as for metallic SWNTs that are missing from the PL empirical fit due to the quenching of the PL signal by metallic SWNTs.

The optical properties of SWNTs are determined by the electronic transitions between van Hove singularities (vHSs) in the density of states (DOS) arising from the one-dimensional (1D) structure of SWNTs. These transition en-

ergies  $E_{ii}$  between vHSs for SWNTs of different structural  $(n, m)$  indices are commonly summarized in the so-called Kataura plot that is widely used in RRS and PL studies of SWNTs.<sup>7</sup> The Kataura plot depicts the  $E_{ii}$  as a function of SWNT diameters ( $d_t$ ) or inverse SWNT diameters ( $1/d_t$ ). For each  $(n, m)$  SWNT,  $d_t = a\sqrt{n^2 + nm + m^2}/\pi$ , where  $a = \sqrt{3}a_{CC}$  is the graphene lattice constant, and  $a_{CC} = 0.142$  nm is the C–C interatomic distance.<sup>1</sup> The  $E_{ii}$  energies in the Kataura plot are arranged in bands ( $E_{11}^S, E_{22}^S, E_{11}^M$ , etc.) for semiconducting (S) and metallic (M) SWNTs, respectively, where the index  $i$  enumerates the vHSs in the valence and conduction bands away from the Fermi level. Within each band in the Kataura plot, the  $E_{ii}$  energies observed from PL measurements follow “family” patterns for SWNTs with  $2n+m=3p+r$ , where  $p$  is an integer and  $r=0,1,2$  define metallic, semiconducting type I (SI) and type II (SII) SWNTs, respectively. The PL empirical fit<sup>6</sup> provides the first two optical transition energies for S SWNTs,  $E_{11}^S$  and  $E_{22}^S$ . When comparing the Kataura plot obtained from the PL empirical fit<sup>6</sup> with the one calculated from the TB approximation,<sup>7</sup> two major differences can be found. First, the experimental  $E_{22}^S/E_{11}^S$  ratio in the large  $d_t$  limit is less than 2, while the tight-binding  $E_{22}^S/E_{11}^S$  ratio approaches 2 with increasing  $d_t$  (the “ratio” problem). Second, the empirical spread of the  $E_{ii}^S$  energies within the same  $2n+m=\text{constant}$  family is much larger than the corresponding spread of the TB  $E_{ii}^S$  energies at constant  $d_t$  (the “family spread” problem). While the “ratio” problem can be explained by many-body effects,<sup>8</sup> the “family spread” is mainly attributed to the curvature effects and to the C–C bond length optimization in smaller  $d_t$  SWNTs,

<sup>a)</sup>Present address: Institute for Solid State Research, Leibniz Institute for Solid State and Materials Research, 01171 Dresden, Germany.

<sup>b)</sup>Electronic mail: millie@mgm.mit.edu

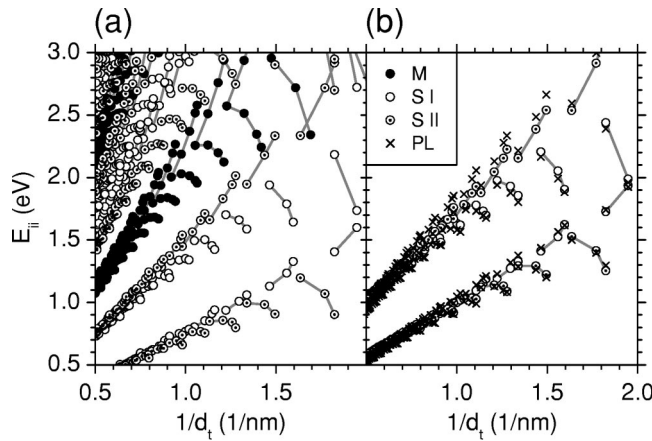


FIG. 1. (a) “Kataura” plot of transition energies  $E_{ii}$  vs inverse diameter  $1/d_t$  for metallic (closed dots) and semiconducting type I (open dots) and type II (marked dots) SWNTs based on the extended tight-binding (ETB) model after geometrical structure optimization. (b) Comparison between the ETB calculations for  $E_{11}^S$  and  $E_{22}^S$  and the PL empirical fit (crosses)—Ref. 6—after making the many-body corrections of Eq. (1).

which are missing from the conventional TB approximation.<sup>1</sup> Meanwhile, it has been shown that long-range interactions of the  $\pi$  orbitals are not negligible,<sup>9</sup> and curvature of SWNT sidewalls yields the  $sp^2$ – $sp^3$  rehybridization in the small  $d_t$  limit. The curvature effect can be included in the TB model, as has been recently reported,<sup>10</sup> by extending the basis set to the atomic  $s$ ,  $p_x$ ,  $p_y$ , and  $p_z$  orbitals that form the  $\sigma$  and  $\pi$  molecular orbitals according to the Slater–Koster formalism.<sup>1</sup> This extended tight-binding (ETB) model utilizes the TB transfer and overlap integrals as functions of the C–C interatomic distance calculated within a density-functional theory (DFT) framework,<sup>11</sup> thus including long-range interactions and bond-length variations within the SWNT sidewall. The atomic  $p$ -orbitals are aligned in the cylindrical coordinates of the SWNT sidewall according to the symmetry-adapted scheme<sup>10</sup> ( $p_z$  is orthogonal to the SWNT sidewall, while  $p_x$  and  $p_y$  are parallel to the SWNT sidewall for each C atom), which allows us to consider an  $8 \times 8$  Hamiltonian for the graphene unit cell of two C atoms (A and B), even for chiral SWNTs with large translational unit cells, thus greatly simplifying the calculations. Furthermore, the total energy of the SWNT can be calculated using the short-range repulsive potential obtained from DFT calculations,<sup>11</sup> and the geometrical structure optimization can then be performed.<sup>10</sup> As shown elsewhere,<sup>10</sup> the resulting optimized SWNT diameter  $d_t^{\text{ETB}}$  slightly exceeds its ideal value  $d_t = a\sqrt{n^2 + nm + m^2}/\pi$ . It is essential to utilize the optimized SWNT structure since the family spread in the Kataura plot is very sensitive to the relaxed atomic positions.

We have used the ETB model<sup>10,11</sup> first to optimize the SWNT structure and then to calculate the vHSs in the DOS of SWNTs and finally to construct the Kataura plot which is shown in Fig. 1(a). By comparing it to the PL empirical fit,<sup>6</sup> we found that the family spread observed in PL studies is closely reproduced by the ETB approximation. The ETB model thus provides the proper chirality dependence for the  $E_{ii}$  energies, since the SWNT chirality changes from armchair-like (A) to zigzag-like (Z) along  $2n+m=\text{constant}$  family lines. The differences between the  $E_{ii}^{\text{PL}}$  energies obtained from PL measurements<sup>6</sup> and the corresponding  $E_{ii}^{\text{ETB}}$  energies calculated from the ETB model, hereafter referred

to as  $\Delta E_{ii}$ , thus weakly depend on the SWNT chirality (generally within the accuracy of PL measurements), while they show a monotonic dependence on  $d_t$ .

These energy differences can be explained by many-body effects, which consist of electron–electron Coulomb repulsion that upshifts  $E_{ii}$  and of the exciton binding that downshifts  $E_{ii}$ .<sup>12</sup> Because of the 1D SWNT structure, electron–electron Coulomb repulsion exceeds the exciton binding so that, overall, many-body  $E_{ii}$  energies are upshifted from one-electron  $E_{ii}$  energies.<sup>12</sup> Since the Coulomb interaction range in SWNTs is of the order of 10 nm,<sup>13</sup> which is much larger than  $d_t$ , the many-body corrections to  $E_{ii}$  are weakly sensitive to the SWNT chirality but essentially only depend on  $d_t$ , on the subband index  $i=1$  or 2, and on the S type I or II. We thus fitted  $\Delta E_{11}^{\text{SI}}$ ,  $\Delta E_{11}^{\text{SII}}$ ,  $\Delta E_{22}^{\text{SI}}$ , and  $\Delta E_{22}^{\text{SII}}$  as functions of  $d_t$  for all  $(n, m)$  SWNTs observed in PL studies.<sup>6</sup> The fit yields

$$\Delta E_{11}^{\text{SI}} = E_{11}^{\text{SI PL}} - E_{11}^{\text{SI ETB}} = (0.15 + 0.11 \text{ nm}/d_t) \text{eV},$$

$$\Delta E_{11}^{\text{SII}} = E_{11}^{\text{SII PL}} - E_{11}^{\text{SII ETB}} = (0.12 + 0.11 \text{ nm}/d_t) \text{eV},$$

$$\Delta E_{22}^{\text{SI}} = E_{22}^{\text{SI PL}} - E_{22}^{\text{SI ETB}} = (0.25 - 0.03 \text{ nm}/d_t) \text{eV},$$

$$\Delta E_{22}^{\text{SII}} = E_{22}^{\text{SII PL}} - E_{22}^{\text{SII ETB}} = (0.31 - 0.03 \text{ nm}/d_t) \text{eV}. \quad (1)$$

We add  $\Delta E_{11}^{\text{S}}$  and  $\Delta E_{22}^{\text{S}}$  given by Eq. (1) to  $E_{11}^{\text{S}}$  and  $E_{22}^{\text{S}}$  calculated in the ETB model, and then plot the resulting  $E_{11}^{\text{S}}$  and  $E_{22}^{\text{S}}$  as a function of  $1/d_t$  in Fig. 1(b). For comparison,  $E_{11}^{\text{S}}$  and  $E_{22}^{\text{S}}$  from the PL empirical fit<sup>6</sup> are also plotted. One can see detailed agreement between the ETB calculations and the PL empirical fit once the many-body corrections of Eq. (1) are taken into account.

The families of  $2n+m=\text{constant}$  bend downward with increasing  $1/d_t$  in the smaller  $d_t$  region, as shown in Fig. 1(b), in full agreement with the PL empirical fit.<sup>6</sup> When using the conventional  $\pi$ -band nearest-neighbor TB approximation, the  $2n+m=\text{constant}$  families never bend down, but rather follow the same general tendency of a linear increase in  $E_{ii}$  as  $1/d_t$  increases. It should be emphasized that when applying the ETB model for the nonoptimized SWNT structure, the calculated family spread is not nearly large enough to fit the spread observed experimentally. This indicates the importance of the geometrical structure optimization on the  $E_{ii}$  values.

To compare the SWNT structures optimized by using the ETB model with the results of other independent geometrical structure optimizations, we plot the change in the C–C bond lengths for each SWNT as a function of curvature ( $1/d_t^2$ ) in Fig. 2. Similar calculations have been performed by Kanamitsu *et al.*<sup>14</sup> for zigzag SWNTs using the DFT framework. Kanamitsu’s bond lengths are also shown for comparison with our calculations. We can see in Fig. 2 that the results of the two independent geometrical structure optimizations agree with each other and follow the same general pattern, yet some deviations are also present [for example, at  $1/d_t^2 = 0.033 \text{ \AA}^{-2}$  for the (7,0) SWNT]. One of the two bond lengths for zigzag SWNTs increases with curvature while the other decreases, in agreement with the physical picture that the optimization process increases the SWNT diameter (from  $d_t$  to  $d_t^{\text{ETB}}$ ) and shrinks the SWNT length. This optimization

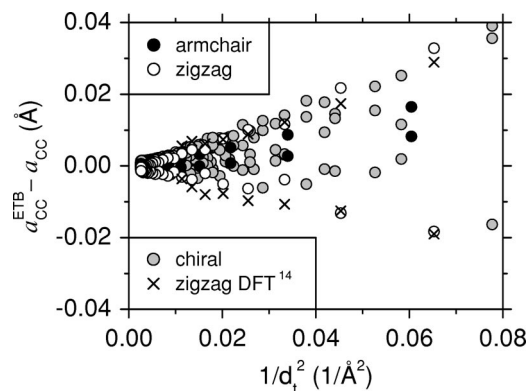


FIG. 2. Differences between the C–C bond lengths  $a_{CC}^{ETB}$  for each SWNT and  $a_{CC}=0.142$  nm in the flat graphene layer as a function of curvature  $1/d_t^2$ . Open, closed, and gray dots denote the bond lengths of zigzag, armchair, and chiral SWNTs, respectively, calculated from the ETB model for the optimized SWNT structures. For comparison, crosses show the bond lengths of zigzag SWNTs from DFT calculations (Ref. 14).

becomes more important as  $d_t$  decreases.<sup>10</sup> The SWNT structures optimized by using the ETB model are thus consistent with other available data.

Once the geometrical structure optimization is performed and the  $E_{ii}$  energies are calculated, we plot them as a function of  $1/d_t$  in the Kataura plot as shown in Fig. 1. However, the Kataura plot used in RRS studies of SWNTs depicts the  $E_{ii}$  energies as a function of  $\omega_{RBM}$ , the radial-breathing mode (RBM) Raman frequency, which is known to vary as  $1/d_t$ .<sup>15</sup> The force-constants for the RBM and other phonon modes can also be calculated for the optimized SWNT structures using the ETB model. The total energy for each SWNT is first calculated and its second derivative is then taken for the atomic displacements along the phonon eigenvector (which corresponds to an increase in  $d_t$  in the case of the RBM) yielding the force-constant for this particular phonon mode. The calculated RBM frequencies  $\omega_{RBM}^{ETB}$  are shown as a function of  $1/d_t$  in Fig. 3. The calculated  $\omega_{RBM}^{ETB}$

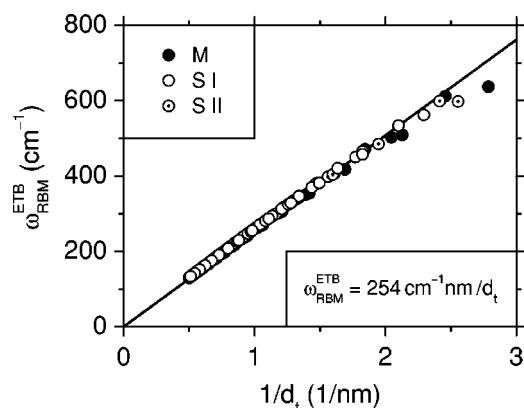


FIG. 3. The radial-breathing mode (RBM) frequencies  $\omega_{RBM}^{ETB}$  for each SWNT as a function of inverse diameter  $1/d_t$ . The frequencies  $\omega_{RBM}^{ETB}$  are calculated from the extended tight-binding (ETB) model for the optimized SWNT structures. Closed, open, and marked dots correspond to metallic, semiconducting type I, and type II SWNTs, respectively. The line shows a linear fit  $\omega_{RBM}^{ETB}=254$   $\text{cm}^{-1}$   $\text{nm}/d_t$  to the calculated points.

follows a linear dependence with  $1/d_t$  up to the smaller  $d_t$  region, where  $\omega_{RBM}^{ETB}$  slightly downshifts from the linear behavior, in agreement with published results.<sup>15</sup> By fitting the calculated  $\omega_{RBM}^{ETB}$ , we obtain  $\omega_{RBM}^{ETB}=254$   $\text{cm}^{-1}$   $\text{nm}/d_t$ . The proportionality coefficient 254  $\text{cm}^{-1}$   $\text{nm}$  is slightly higher than the values observed experimentally in RRS studies of SWNTs (223–248  $\text{cm}^{-1}$   $\text{nm}$  for different samples<sup>2,4,5</sup>). The calculated force-constants are generally upshifted from experimental values according to the variational principle. Thus the  $\omega_{RBM}$  calculated from first principles should generally be scaled down by  $\sim 10\%$ . Such scaling brings the calculated  $\omega_{RBM}^{ETB}$  down to the experimental range of the observed  $\omega_{RBM}$ . Using the proper RBM proportionality coefficient for a specific SWNT sample, the Kataura plot in Fig. 1 can be redrawn as a function of  $\omega_{RBM}$  for its practical use in RRS studies. Furthermore, the geometrical structure optimization can be performed in the presence of different SWNT wrapping agents, thus allowing us to predict theoretically the observed changes in the  $E_{ii}$  energies for different SWNT samples.

In summary, a theoretical basis is provided in support of the PL empirical fit<sup>6</sup> for the optical transition energies in SWNTs. The model may be extended with future experiments to a wider SWNT diameter range, to other electronic subbands beyond  $E_{11}^S$  and  $E_{22}^S$ , to metallic SWNTs not seen in PL studies, and to experimental SWNT samples containing a variety of surfactants and wrapping agents, and whether or not SWNTs are suspended, or are on particular substrates, and whether the SWNTs are solvated or not.

The MIT authors acknowledge support under NSF Grant No. DMR 04-05538. The Tohoku U. authors acknowledge a Grant-in-Aid (Nos. 13440091 and 16076201) from the Ministry of Education, Japan. A.J. acknowledges financial support from CNPq-Brazil (Profix).

<sup>1</sup>R. Saito, G. Dresselhaus, and M. S. Dresselhaus, *Physical Properties of Carbon Nanotubes* (Imperial College Press, London, 1998).

<sup>2</sup>A. Jorio, R. Saito, J. H. Hafner, C. M. Lieber, M. Hunter, T. McClure, G. Dresselhaus, and M. S. Dresselhaus, *Phys. Rev. Lett.* **86**, 1118 (2001).

<sup>3</sup>M. Ouyang, J. L. Huan, C. L. Cheung, and C. M. Lieber, *Science* **292**, 702 (2001).

<sup>4</sup>A. G. Souza Filho, S. G. Chou, G. G. Samsonidze, G. Dresselhaus, M. S. Dresselhaus, L. An, J. Liu, A. K. Swan, M. S. Ünlü, B. B. Goldberg, A. Jorio, A. Grüneis, and R. Saito, *Phys. Rev. B* **69**, 115428 (2004).

<sup>5</sup>S. M. Bachilo, M. S. Strano, C. Kittrell, R. H. Hauge, R. E. Smalley, and R. B. Weisman, *Science* **298**, 2361 (2002).

<sup>6</sup>R. B. Weisman and S. M. Bachilo, *Nano Lett.* **3**, 1235 (2003).

<sup>7</sup>H. Kataura, Y. Kumazawa, Y. Maniwa, I. Umezue, S. Suzuki, Y. Ohtsuka, and Y. Achiba, *Synth. Met.* **103**, 2555 (1999).

<sup>8</sup>C. L. Kane and E. J. Mele, *Phys. Rev. Lett.* **90**, 207401 (2003).

<sup>9</sup>S. Reich, J. Maultzsch, C. Thomsen, and P. Ordejón, *Phys. Rev. B* **66**, 035412 (2002).

<sup>10</sup>V. N. Popov, *New J. Phys.* **6**, 17 (2004).

<sup>11</sup>D. Porezag, T. Frauenheim, T. Köhler, G. Seifert, and R. Kaschner, *Phys. Rev. B* **51**, 12947 (1995).

<sup>12</sup>T. Ando, *J. Phys. Soc. Jpn.* **66**, 1066 (1997).

<sup>13</sup>C. D. Spataru, S. Ismail-Beigi, L. X. Benedict, and S. G. Louie, *Phys. Rev. Lett.* **92**, 077402 (2004).

<sup>14</sup>K. Kanamitsu and S. Saito, *J. Phys. Soc. Jpn.* **71**, 483 (2002).

<sup>15</sup>J. Kürti, V. Zólyomi, M. Kertesz, and G.-Y. Sun, *New J. Phys.* **5**, 125 (2003).